Title

Solar Desalination Using Thermally Responsive Ionic Liquids Regenerated with a Photonic Heater

Journal

Environmental Science and Technology, 55(5)

ISSN

0013-936X

Authors

Haddad, Andrew Z
Menon, Akanksha K
Kang, Hyungmook
et al.

Publication Date

2021-03-02

DOI

10.1021/acs.est.0c06232

Peer reviewed

Solar Desalination using Thermally Responsive Ionic Liquids Regenerated with a Photonic Heater

Andrew Z. Haddad,[1]† Akanksha K. Menon,[1]† Hyungmook. Kang,[2,3] Jeffrey J. Urban,[2] Ravi S. Prasher,[1,3] Robert Kostecki[1]**

[1] Energy Storage and Distributed Resources Division, Lawrence Berkeley National Laboratory, Berkeley, CA, 94720, USA.

[2] Molecular Foundry, Lawrence Berkeley National Laboratory, Berkeley, CA, 94720, USA.

[3] Department of Mechanical Engineering, University of California, Berkeley, CA, 94720, USA.

† These authors contributed equally to this work.

* Corresponding authors: r_kostecki@lbl.gov, rsprasher@lbl.gov.

ABSTRACT

Growing global water demand has brought desalination technologies to the forefront for freshwater production from non-traditional water sources. Among these, forward osmosis (FO) is a promising two-step desalination process (draw dilution and regeneration), but it is often overlooked due to the energetic requirements associated with draw regeneration. To address this limiting factor, we demonstrate FO desalination using thermally responsive ionic liquids (ILs) that are regenerated using a renewable energy input, *i.e.*, solar heat. To efficiently harness sunlight, a simple photonic heater converts incoming irradiation into infrared wavelengths that are directly absorbed by IL-water mixtures, thereby inducing phase separation to yield clean water. This approach is markedly

different as it uses radiative heating, a noncontact mode of heat transfer that couples to chemical functional groups within the IL for rapid energy transfer without a heat exchanger or secondary fluid. Overall, a solar-thermal separation efficiency of 50% is achieved under unconcentrated sunlight, which can be increased to 69% with thermal design. Successful desalination of produced water from oil wells in Southern California highlights the potential of solar powered IL-FO for energy-efficient and low cost desalination of complex brines for beneficial water reuse.

Keywords. Water-energy nexus, solar heat, stimuli-responsive materials, photo-thermal converter, produced water, wastewater treatment, renewable desalination, forward osmosis

INTRODUCTION

Global water demand is projected to increase by 55% over the next three decades owing to population growth, industrialization and climate change.[1-2] Concomitantly, large volumes of wastewater and concentrate are discharged from municipal, agricultural and industrial processes and their disposal has a significant environmental impact. These non-traditional brines are far more varied in their salinity and composition than seawater, thereby requiring new treatment methods beyond reverse osmosis (RO).[3] For example, produced waters, a byproduct of oil and gas extraction, represent an underutilized water resource – in the United States alone, nearly one million oil and gas wells generate ~2.4 billion gallons of water per day.[4] This water is typically disposed by deep-well injection, but increased environmental regulation and economic incentives are pushing industry to explore treatment options that convert produced water into a value added commodity, *e.g.* water for agricultural reuse.

Forward osmosis (FO) is a promising technology for desalination of non-traditional waters and complex brines due to a number of intrinsic benefits over other technologies.[5] Recent literature has shown that FO exhibits a higher fouling and scaling resistance relative to RO,[6-7] making it suitable for variable water composition with minimal pre-treatment and membrane maintenance and/or replacement.[8-9] In FO, the osmotic pressure difference between a saline solution (feed) and a higher concentration solution (draw) causes water to spontaneously diffuse across a semi-permeable membrane until osmotic equilibrium is attained by diluting the draw. Traditional draw solutes comprise inorganic salts (*e.g.* sodium chloride) that generate large osmotic pressures at high molar concentrations and yield favorable water fluxes. However, osmotic strength is not the only factor for draw selection, as FO requires a second step to regenerate the draw and produce clean water, which is very energy intensive. For example, sodium chloride can be recovered either by supplementing FO with RO that requires more electrical energy than direct treatment (*i.e.*, RO without FO) of the same feed,[10] or by evaporating water using thermal or membrane distillation that is constrained by the large enthalpy of vaporization of water (~2400 J g^{-1}).[11-12] Such energy-intensive processes for regeneration of inorganic draws have thus far precluded FO as a competitive desalination technology. However, FO has the ability to utilize low-grade or waste heat sources for draw regeneration, provided that a suitable draw solution is used. Thus, identifying a chemistry that satisfies both criteria of high osmotic pressure for water flux, as well as an energy-efficient regeneration mechanism represents a key challenge.

A novel class of draw solute materials are thermo-responsive ionic liquids (ILs), pioneered by Ohno and coworkers,[13-14] which were originally developed for protein extraction from aqueous solutions. The inherent ionic state of these organic salts generates high osmotic pressures that enables their use as draws for FO.[15-16] Furthermore, aqueous mixtures of these ILs exhibit a liquid-liquid phase

separation when heated above a critical temperature (lower critical solution temperature or LCST) owing to a negative entropy of mixing. The energy required for separation of water from ILs (*i.e.*, enthalpy of de-mixing) is approximately 10 J g^{-1}, which is orders of magnitude lower than the first order phase transition of water that is prevalent in traditional thermal regeneration (2400 J g^{-1}). This liquid-liquid phase separation is also much simpler than other draws used in FO with solubility-dependent regeneration mechanisms that evolve gases,[17-18]and it occurs at relatively low temperatures <50 °C and at atmospheric pressure. As a result, these thermo-responsive draw solutions can be coupled with a low-grade source such as solar-thermal energy, which in turn significantly reduces the carbon footprint and cost of water treatment.[2] Despite this, IL-water phase separation has not received much attention, with literature being limited to heating a beaker immersed in a water bath or a hot plate for draw regeneration.[16, 19] Furthermore, IL-based FO has only been tested with simple NaCl feed solutions, and the use of custom-synthesized membranes have limited its practical use.[15-16]

In this work, we demonstrate a proof-of-concept comprising LCST-type ILs as draw solutions for FO desalination coupled to a solar energy harvester that provides heat for regeneration. Solar energy can either be harnessed indirectly (absorbed by a solid surface or a heat transfer fluid in a conventional solar collector) or directly *via* absorption by the liquid. In the first case, a heat exchanger may be required to transfer heat to the draw, which not only has surfaces that are susceptible to corrosion over time, but also adds to the overall system cost. In contrast, direct absorption of energy by the liquid is an efficient and noncontact mode of heating that depends predominantly on the spectral optical properties of IL-water mixtures, which have not been measured to date. Herein, we demonstrate the feasibility of this new approach using a photo-thermal device (*aka* photonic heater) that enables radiative heating. The overarching goal is the

development of a continuous process in which the thermo-responsive IL effectively draws water in an FO membrane unit and then undergoes regeneration in a thermal separator unit, thereby providing high quality freshwater (total dissolved solids, TDS <500 ppm) with minimal electrical energy input, as shown in Fig. 1.

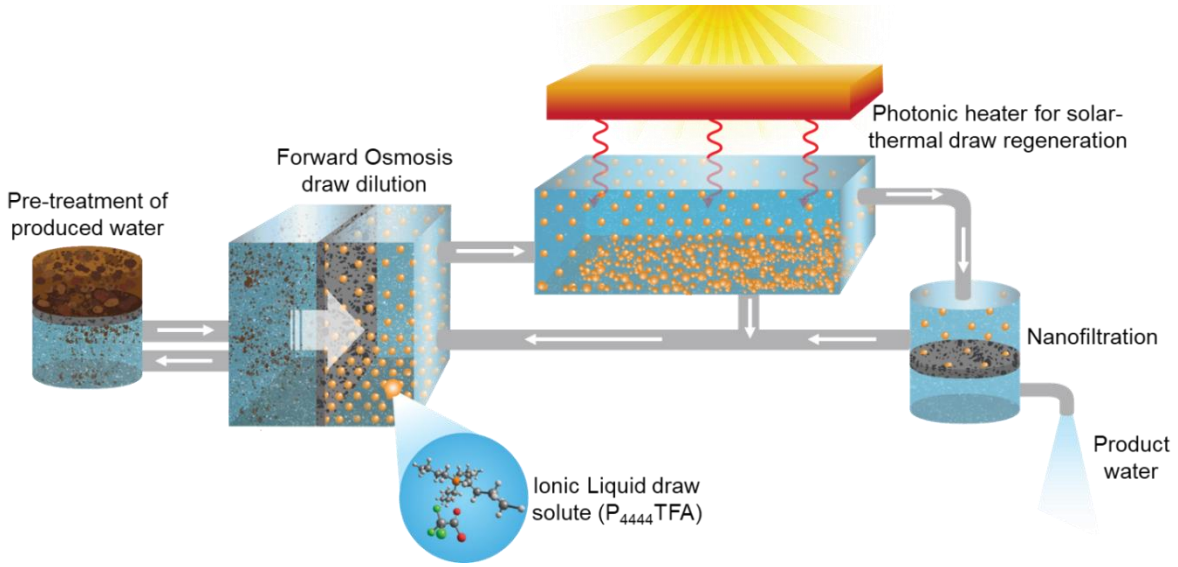

Fig. 1. An illustration of the proposed solar-FO desalination system. A contaminated feed *(e.g.* produced water from oil and gas extraction) undergoes pre-treatment and enters an FO membrane module in which the IL draw solute (with a higher concentration compared to the feed) causes water molecules from the feed to diffuse through the membrane under a natural osmotic gradient. The diluted draw then flows into a thermal separator in which thermal emission from the photonic heater illuminated by sunlight causes a rise in its temperature. Liquid-liquid phase separation occurs as the temperature increase above LCST, with the denser IL-rich phase settling at the bottom while the water-rich phase is on top. The former is recycled as the draw for FO, while the water-rich phase with residual IL content undergoes a low pressure nanofiltration polishing step to attain high quality product water.

MATERIALS AND METHODS

Various thermo-responsive ILs have been identified in literature for different applications, but not all are suitable for solar-FO desalination. With multiple properties to be optimized and many

potential IL chemistries, the analytical hierarchy process[20] was used to down-select suitable ILs. Specifically, ILs with tetrabutylphosphonium (P_{4444}^+) as the cation were chosen as its amphiphilicity results in LCST behavior with a variety of anions; with 2,4-dimethylbenzene sulfonate (P_{4444}DMBS or DMBS) and trifluoroacetate (P_{4444}TFA or TFA) emerging as ideal candidate materials (table S1).

Synthesis of Ionic Liquids. P_{4444}DMBS was synthesized using a neutralization reaction.[15] The starting materials were tetrabutylphosphonium hydroxide (TBPH) and 2,4-dimethylbenzene-sulfonic acid (TCI America). Both reagents were mixed with water in a 1:1 molar ratio, with a slight excess of the sulfonic acid and stirred at room temperature for 24 hours. The solution was then added to a separatory funnel and extracted with dichloromethane (DCM); this step was repeated three times. The organic phase was collected and washed with water three times and then transferred to a rotary evaporator in order to remove DCM from the IL. The resultant IL was stored in a vacuum oven at 90 °C for 48 hours to remove residual water. ^{1}H-NMR spectra of P_{4444}DMBS in *d*-DMSO (δ/ppm relative to TMS) showed: δ = 0.81-0.93 (12H; a), 1.29-1.54 (16H; b, c), 2.05-2.18 (8H, d), 2.18 (3H, g), 2.45 (3H, e), 6.78-6.94 (2H; f, h), 7.52-7.61 (1H, i); see fig. S1A. P_{4444}TFA was also prepared using a neutralization reaction between TBPH and trifluoroacetic acid (TCI America). TBPH was added to water and stirred, and trifluoroacetic acid was added drop-wise to this solution over several hours and mixed at room temperature for 24 hours. The solution was then worked up using DCM extraction and dried in the vacuum oven, as described for DMBS. ^{1}H-NMR was performed (DMSO, δ/ppm relative to TMS): δ = 0.78-0.98 (3H; a), 1.25-1.51 (4H; b,), 2.03-2.19 (2H, c); see fig. S1B.

Characterization of Ionic Liquid Solutions. Relevant solution properties of aqueous mixtures of ILs were characterized as a function of concentration.

Phase diagram: To obtain the LCST of the ionic liquids, UV-Vis spectroscopy was performed (Agilent Technologies). Cloud point measurements[21] were used to identify the temperature at which the transmittance drops from 100 to 0%, *i.e.*, the point where phase separation is initiated. (fig. S2). Differential scanning calorimetry (DSC) was performed to verify the temperature at which phase separation occurs and to measure the enthalpy of transition (fig. S3).

Viscosity: Aqueous IL solutions were measured using an HR-2 rheometer (Discovery Series from TA Instruments) with a parallel plate accessory at a shear rate of 100 Hz. Measurements at 25 °C of 40 wt % P_{4444}DMBS confirmed the Newtonian behavior for this class of phosphonium ionic liquids (fig. S4). A thermostatted Peltier accessory was used to measure temperature-dependent viscosity, with a resolution of 0.1 °C.

Osmotic pressure: To evaluate the osmotic strength, osmolality was measured using a Wescor 5600XR vapor pressure osmometer (Thermo Fisher Scientific). Osmolality was converted to an approximate osmotic pressure, π as: $\pi = m\rho RT$, m is the measured osmolality, ρ is the density of the mixture (approximated as the density of water), R is the molar gas constant, and T is the absolute temperature.

Optical properties: UV-Vis spectroscopy and FTIR-ATR (Thermo Electron Nicolet 5700) were used to measure the optical properties of pure ILs over a wide wavelength range. Optical properties of IL-water mixtures in the infrared region were measured in transmission mode using an Omni-Cell liquid accessory (Specac) with KRS-5 windows and a fixed path length of 50 μm (fig. S14). Optical properties of the photonic heater comprising a selective solar absorber (TiNOX, Almeco Group) and blackbody emitter (Zynolyte hi-temp paint, Aervoe) were also measured using an FTIR with an integrating sphere accessory (Pike Technologies Mid-IR IntegratIR). As the samples were non-transmitting, absorptance was calculated as unity minus reflectance (fig. S15).

Membrane Characterization. An FEI Phenom tabletop Scanning Electron Microscope (SEM) was used to obtain high resolution images of new and used membranes post-FO experiments with ionic liquids and produced water samples, and EDX maps of the active and support layer of the membrane were generated (fig. S11-S13).

Forward Osmosis Draw Dilution Process. FO experiments were performed in a lab-scale setup comprising a commercial acrylic cross-flow cell (Sterlitech Corporation) at 25 °C using a thin film composite membrane (Porifera Inc.). Feed and draw solutions were pumped in counter-current mode at 200 mL min^{-1} (crossflow velocity ~3 cm s^{-1}). The feed was placed on an analytical balance to measure mass loss over time ($\Delta m/\Delta t$), and water flux was calculated as: $J_w = \frac{\Delta m/\rho}{A_m \Delta t}$, where A_m is the effective membrane area (fig. S9). Active layer facing the draw resulted in higher water fluxes, and this configuration was used for all experiments. The reverse solute flux was obtained using a conductivity probe (for NaCl) and by performing a Total Organic Carbon analysis (for ILs) to measure changes in feed concentration over time ($\Delta C/\Delta t$) as: $J_s = \frac{\Delta C \times \Delta m/\rho}{A_m \Delta t}$. Long duration experiments were conducted for 16 hours with continuous draw dilution (fig. S10B).

Solar-Thermal Draw Regeneration Process. A solar simulator (Newport, 94081A) with an optical filter for AM 1.5G spectrum was used. A power meter and thermopile detector (Newport, 919P-030-18) were used to measure the incoming solar flux (1000 W m^{-2}) at the same location as the diluted draw. The draw was placed in an acrylic vessel, which comprises an inner pocket (square with a side length of 3.5 cm and a 5 cm depth) coated in reflective foil. The inner pocket is surrounded by a 2 cm thick acrylic wall on all sides to minimize thermal losses. K-type thermocouples were placed at 0.5 cm and 4 cm below the liquid surface to record the temperature at the top (T_{top}) and bottom of the vessel (T_{bottom}), respectively. The photonic heater was placed ~4 mm above the liquid to ensure a high view factor for noncontact radiative heat transfer. A K-type

thermocouple on the surface of the photonic heater measured its temperature to estimate the blackbody emissive power. The thermocouples were connected to a data logger (Pico Technologies, USB TC-08).

Nanofiltration Post-treatment Process. A dead-end filtration stainless steel stirred cell was used (Sterlitech Corporation) with a 47 mm diameter membrane disc (Dow Filmtec). The NF270 polyamide membrane with a molecular weight cutoff of 200-400 Da was chosen as it is designed to remove organics, thereby making it suitable for rejection of ionic liquids. To minimize concentration polarization at the membrane surface, a PTFE-coated magnetic stir bar was used at 200 rpm. The cell was connected to a nitrogen cylinder using a pressure gauge and the resulting water flux, J_w was obtained by measuring the change in permeate volume over time.

Evaluation of Non-Ideal Mixture Behavior *via* Molecular Dynamics (MD) Simulations. All-atom AMBER force fields for potential energy, U were used in the MD simulation of this system.

$$U_{potential} = \sum_{i>j}\left[4\varepsilon_{ij}\left\{\left(\frac{\sigma_{ij}}{r_{ij}}\right)^{12}-\left(\frac{\sigma_{ij}}{r_{ij}}\right)^{6}\right\}+\frac{q_i q_j}{4\pi\varepsilon_0\varepsilon_r r_{ij}}\right]+\sum_{bonds}K_r(r-r_0)^2+\sum_{angles}K_\theta(\theta-\theta_0)^2 + \sum_{torsions}\frac{K_\varphi}{2}\{1+\cos(n\phi-\gamma)\} \quad (1)$$

The first term describes the non-bonded interactions including Van der Waals as the Lennard-Jones 12-6 form and Coulombic forces from atom-centered partial charges. The following terms in the potential energy equation represent, respectively, bonds, angles and torsional interactions. The force field parameters of atomistic P_{4444} cation, DMBS anion and TFA anion were developed in previous work[22-24] (tables S3-S6). The TIP4P water model[25] was employed for water molecules, which depicts the dynamic and structural properties of liquid water. The VdW interaction parameters between unlike atoms were obtained from the Lorentz−Berthelot combining rule. Non-

bonded interactions separated by exactly three consecutive bonds (1−4 interactions) were reduced by related scaling factors,[26-27] which were optimized as 0.50 for VdW interactions and 0.83 for electrostatic interactions, respectively. The schematic molecular structures and partial charges of the P_{4444} cation, DMBS anion, TFA anion and water molecule of the TIP4P water model are presented in fig. S5. Atomic charges for DMBS anion were calculated using a web-based calculator, Atomic Charge Calculator, via the Electronegativity Equalization Method (EEM).[28] MD simulation was performed using LAMMPS package with standard 3D periodic boundary conditions. The number of initially displayed ion pairs and water molecules to match the concentration cases is summarized in table S7. The non-bonded interactions were cut off at 15 Å while the particle-particle particle-mesh solver[29] was applied to treat the long-range electrostatic interactions. All simulations were carried out at isothermal-isobaric conditions, at 25 °C and ambient pressure, in the Nose-Hoover NPT ensemble with time coupling constants of 100 and 1000 fs, respectively. After initial relaxations with short time steps and an equilibration with long time steps, at least 6 ns simulation of the ensemble were performed with a fixed time step of 1fs. Atomic simulation trajectory or RDFs were recorded at an interval of 1.5 ps for post-analysis.

RESULTS AND DISCUSSION

Solution Properties of Thermo-Responsive ILs. The binary phase diagram and critical transition temperature of both DMBS and TFA are shown in Fig. 2A. DMBS displays a broad binodal phase curve, with an LCST of 36 °C at a concentration of 40 wt%, while the TFA phase curve is symmetric with an LCST of 31 °C at that concentration. The curve width dictates the effectiveness of phase separation upon heating - at a temperature of 55 °C, the 40 wt% DMBS separates into a concentrated IL-rich phase >80 wt%, while TFA at the same concentration and temperature separates into an IL-rich phase of ~70 wt% (confirmed by NMR analysis). Thus, the

draw solutions should be heated not just to their LCST, but to temperatures ~20 °C higher in order to be regenerated and reused in a subsequent FO process, while the water-rich phase contains <10 wt% IL. The enthalpy of separation or de-mixing, ΔH_{mix}, for both ILs at a concentration of 50 wt% was obtained as 2-5 J g^{-1} of the mixture (fig. S3). This liquid-liquid separation enthalpy is 1000x lower than the enthalpy of liquid-vapor phase change, which highlights advantages of using these ILs that undergo a reversible phase separation with water.

The viscosity of DMBS and TFA solutions are shown in Fig. 2B, as viscous draws can cause concentration polarization that adversely impacts water flux.[30] At concentrations <30 wt% the mixture viscosity is close to that of water (~1 mPa-s) but then increases with concentration, likely due to molecular interactions (*e.g.* ion pairing and/or molecular aggregation) at non-dilute concentrations.[31] These molecular interactions also result in an unusual dependence of viscosity on temperature: as the IL-water mixture is heated above room temperature, its viscosity decreases according to the well-known Arrhenius relationship. However, as the critical temperature for a given concentration is approached, viscosity increases sharply, indicating structural reorganization and formation of aggregates in solution that leads to phase separation. With further increase in temperature, viscosity decreases again as the phase-separated water-rich layer resembles a dilute mixture (fig. S4). Similar temperature-dependent viscosity trends have been reported in binary mixtures of water and imidazolium-based ILs that do not display LCST behavior, as well as in LCST-type polymers or polyelectrolytes in which aggregation increases the effective molecular weight, thereby showing a sharp increase in viscosity with temperature.[32-33] In contrast, the lower viscosity of the two down-selected ILs (at least by a factor of three) at all concentrations, as well as their weaker temperature dependence around the critical temperature is more suitable for FO.

To evaluate the ability of ILs as draw solutes to desalinate saline feeds, their osmotic strength was measured at different concentrations. We note that these measurements were performed at 25 °C (temperature at which FO dilution occurs), which is in contrast with literature measurements based on freezing point that over-predicts osmotic strength as the physical state of the mixture and thermal interactions are altered at low temperatures.[16] Fig. 2C shows the osmolality of both ILs, which provides a measure of ions dissolved in solution at a given concentration, and this is converted into an approximate osmotic pressure. The osmotic pressure of both ILs can be tuned by changing the mixture concentration, rendering them suitable for salinities ranging from brackish water to produced water. At low concentrations <10 wt%, the osmolality of both DMBS and TFA increase linearly, indicating complete dissociation into constituent ions as expected in a dilute mixture. However, at intermediate concentrations ~20-50 wt%, both ILs appear to have a near-constant osmolality, which increases dramatically upon further increase in concentration >60 wt%.

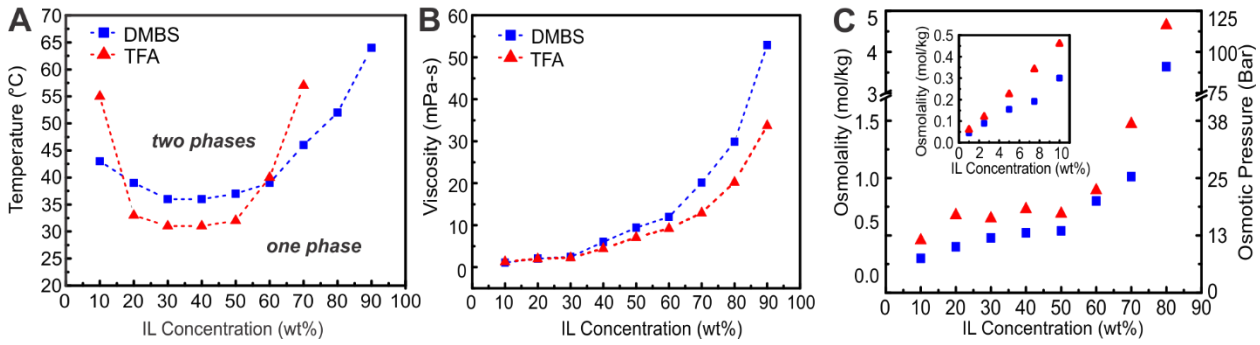

Fig. 2. Characterization of aqueous mixtures of DMBS (in blue) and TFA (in red) as a function of their concentration in water. (A) Binodal phase diagram that shows the LCST **(B)** Viscosity. **(C)** Osmolality and calculated osmotic pressure, with dilute mixtures shown in the inset.

To understand this unusual behavior, osmolality was plotted as a function of mixture molality and compared with an ideal solute like NaCl. As shown in Fig. 3A, above ~0.3 mol kg^{-1}, osmotic pressure generated by IL ions in solution deviates significantly from NaCl dissolved in water. To

provide insight on this, Molecular Dynamics (MD) simulations were performed, in which the parameter of interest is the number of water molecules in the first hydration shell of the IL that is known to be a prerequisite for LCST behavior (Supplementary Note S2).[31] The first peak of the radial distribution function between atoms in the IL and water provides information on atoms that constitute hydration shells and their radius – the central P atom in the P_{4444} cation, S atom and benzene ring in the DMBS anion, and the C2 atom in the TFA anion were pivots for hydration shells (fig. S6-S7). The inset in Fig. 3B provides a pictorial representation for DMBS showing the distribution of water molecules *(i)* exclusively within the coordination shell of a single ion, *(ii)* shared between multiple ions, or *(iii)* outside the first coordination shell of all ions. As the IL concentration increases, the number of water molecules inside the first coordination shell per ion pair decreases (Fig. 3B line graph). Furthermore, the ratio of water molecules contributing to the first coordination shell of multiple ions increases at higher IL concentrations (Fig. 3B area graph). In other words, not all individual ions are hydrated due to an insufficient number of water molecules at these high concentrations of DMBS, resulting in ion aggregation and shared water molecules between multiple ions. The following hypothesis was tested: to contribute to osmotic strength, a certain number of water molecules are required at a given concentration for IL dissociation into its constituent ions (*i.e.,* one cation and one anion per IL molecule). Single cation and anion simulations were performed to calculate the number of water molecules in the ions' first coordination shell that ensure dissociation (fig. S8). Given that water molecules are shared by multiple ions at some concentrations, two definitions of free ion were evaluated: shared water molecules solvate all ions, or only solvate the nearest ion. Simulation results for both ionic liquids indicate that the latter definition dominates, *i.e.,* shared water molecules contribute only to solvating the nearest ion, as this correlates well with experimental data shown in Fig. 3C for

DMBS. The apparent free ion ratio is defined as the ratio of measured osmolality to that predicted by van't Hoff theory for an ideal solute that dissociates into two ions (*i.e.*, like NaCl) in solution. This suggests that a number of IL ions in solution are clustered, with shared hydration shells solvating only the nearest ion which hinders other ions from contributing to osmotic strength. At all concentrations, TFA has a larger free ion ratio than DMBS as shown in Fig. 3D, resulting in a higher osmolality.

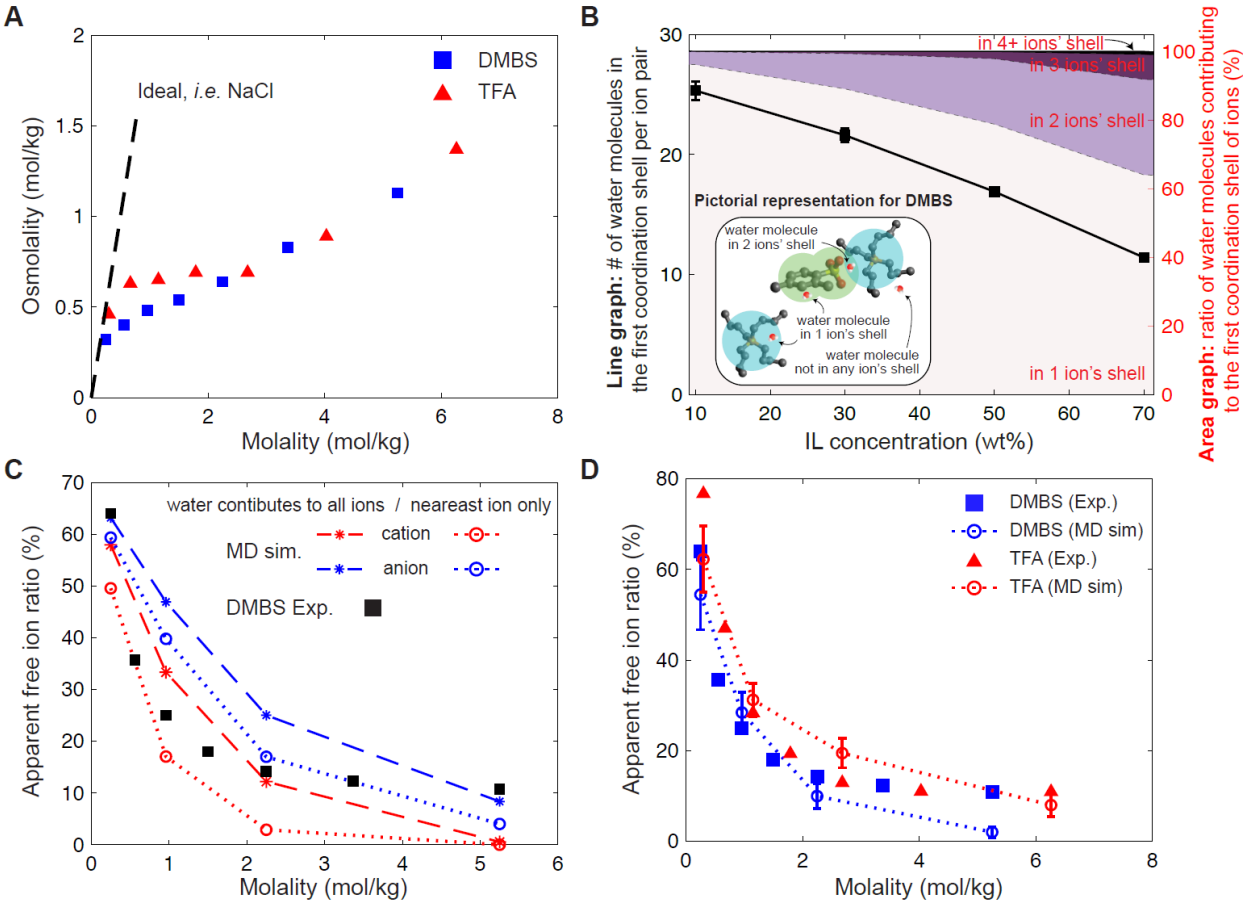

Fig. 3. Concentration dependence of osmolality showing deviations from ideal mixtures. (A) Osmolality measured as a function of molality using a vapor pressure method showing differences between ILs and NaCl in solution. **(B)** Molecular dynamics simulation showing the number of water molecules in the first coordination shell per ion pair of DMBS (line graph) and the ratio of water molecules contributing to the first coordination shell of multiple ions (area graph) as a function of IL concentration **(C)** Molecular dynamics simulation showing the apparent free cation and anion ratio for DMBS compared to experimental data under

two assumptions. **(D)** Molecular dynamics simulation showing the apparent free ion ratio for DMBS (in blue) and TFA (in red) compared to experimental data under the hypothesis that water molecules contribute to the osmotic strength of the nearest ion only.

The osmolality data and MD simulations reveal for the first time, the existence of a critical concentration that is unique to each IL. This concentration represents the point at which IL-water mixtures deviate from ideality and behave like complex (*i.e.*, non-dilute) fluids with ion pairing that results in a lower osmotic pressure and adversely impacts FO water flux. We have previously shown that ion aggregation is dependent on temperature and is an intermediate step towards LCST-type phase separation,[31] but the occurrence of aggregation at room temperature is revealed for the first time through these MD simulations. This indicates an opportunity to develop new IL chemistries that exhibit higher critical concentrations for aggregation (*i.e.*, less ion pairing like TFA compared to DMBS) to ensure higher osmotic pressures.

Forward Osmosis Desalination of Produced Water Feeds. A lab-scale FO setup was designed to test the performance of the two IL draw solutions, as shown in Fig. 4A. Commercially available FO membranes are benchmarked against traditional inorganic draw solutions like NaCl using water flux (in L m^{-2} h^{-1} or LMH) and reverse solute flux, RSF (in g m^{-2} h^{-1} or gMH) with a deionized water feed. RSF is a measure of draw solute back-diffusion through the membrane that gradually lowers draw concentration (and increases feed concentration), thereby decreasing the water flux and requiring periodic draw replenishment that increases operational costs.[34] Given the differences in solution properties of ILs and simple salts like NaCl, the selectivity of commercial FO membranes with ILs was tested. Fig. 4B displays the measured water flux using 70 wt% DMBS and TFA draws with a DI water feed, and the corresponding RSF. The membrane selectivity, γ is obtained by dividing reverse solute flux by the water flux across the membrane.[35] DMBS and TFA IL-based draws show γ values of 0.18 and 0.05 g L^{-1}, respectively, which are lower than NaCl (0.7

g L^{-1}) and also significantly lower than other thermally regenerated draws such as ammonia-carbon dioxide (γ >2 g L^{-1}).[35] This is attributed to the larger size of the IL molecules (12.5 Å unhydrated) compared to NaCl (5.6 Å unhydrated), which hinders back diffusion of the IL through the FO membrane. While DMBS and TFA IL-based draws exhibit low RSFs relative to other FO draws, this draw leakage will necessitate periodic draw replenishment over time. Efforts directed at optimizing flow parameters and membrane design will aid in reducing RSF values further. These results confirm that commercial membranes used in this work show a high selectivity with organic solutes, indicating that the selected LCST-type draws are suitable for FO.

To evaluate the use of ILs in a practical application, real produced water feeds were obtained from two different oil fields operated by the California Resources Corporation (Elk Hills and South Mountain) in southern California (table S2). Based on the measured osmolality of produced water samples, 70 wt% TFA and 70 wt% DMBS draw solutions were selected. Fig. 4C shows the desalination performance of both IL-based draws, with TFA yielding a higher water flux owing to its higher osmolality and lower viscosity when compared to DMBS at the same concentration. We note that the flux values can be increased significantly by lowering mass transport resistances, *e.g.* higher cross-flow velocities (compared to ~3 cm s^{-1} used in these experiments) and well-designed hydrodynamics in custom-designed cells (using spacers and shims), and should be considered to realize the full potential of IL chemistries as draws in FO.

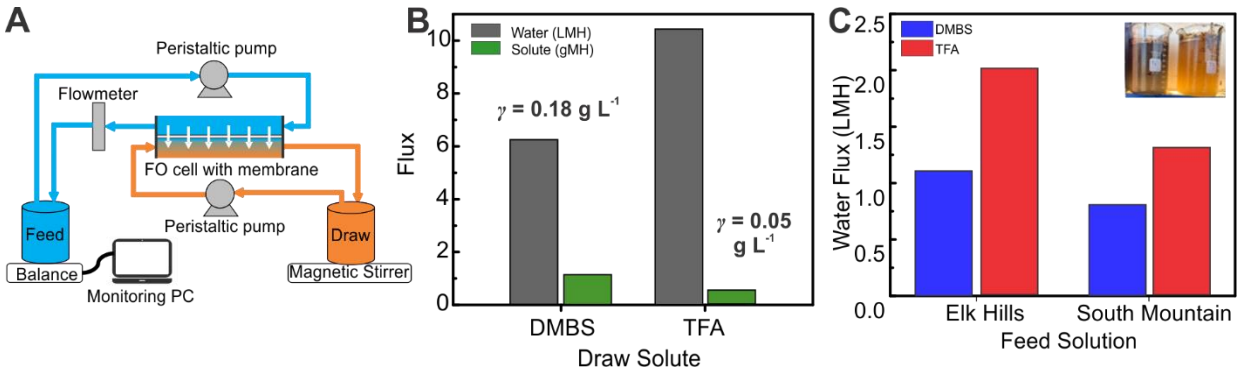

Fig. 4. Lab-scale forward osmosis experiments. (A) Schematic of the experimental FO setup to evaluate the water flux for different feed and draw solutions. The membrane is oriented such that the active layer faces the draw in all experiments. **(B)** Measured water flux (LMH) and reverse solute flux (gMH) when using IL-based draw solutes, 70% DMBS and 70% TFA, with a DI water feed; γ represents the membrane selectivity and is obtained by dividing the solute flux by the water flux. **(C)** Measured water flux using real produced water samples (Elk Hills, South Mountain) with 70% DMBS and 70% TFA as draw solutes. The inset shows the feed samples used in the FO process (courtesy of the California Resources Corporation).

To assess the compatibility of commercial membranes with IL draws and produced water feeds, SEM-EDX analysis was performed. The structural (fig. S11) and chemical (fig. S13) composition of the membrane remain unchanged, thereby confirming that commercial FO membranes can be reused after rinsing or backwashing with DI water, with no significant decrease in flux over multiple runs with the ILs and produced water feeds (table S8).

Draw Regeneration and Clean Water Production using Solar Heat. After the FO step, diluted draw solutions ~40-50 wt% (based on NMR analysis) must undergo phase separation by heating above the LCST. Solar energy is used as the heat source, with the goal of achieving direct absorption of radiation by the liquid to increase its temperature. This noncontact mode of heating proceeds *via* thermal radiation and has advantages over conventional photo-thermal materials and surfaces that heat the liquid *via* convection and/or conduction, which is limited to lower temperatures and is susceptible to corrosion or degradation over time.[36-37] However, pure ILs are transparent across the solar spectrum (fig. S14A) and instead show multiple absorption bands in the infrared that correspond to vibration modes of constituent chemical functional groups (Supplementary Note S4). Given that water's O-H bond strongly absorbs at *ca*. 2.8 μm, it is expected that IL-water mixtures will also absorb across the IR region. Fig. 5A shows the infrared transmittance of 50 wt% DMBS and TFA; the transmittance of DI water is also measured and

matches literature data.[38] For both mixtures, strong absorption in the short- (2.5-3 μm) and mid-infrared (6-8 μm) wavelength range corresponds to vibrational and rotational modes of the pure IL molecules (fig. S14B). Thus, by converting solar energy into infrared radiation, direct absorption by the liquid can induce effective phase separation, *i.e.*, draw regeneration. This is achieved using a photonic heater that absorbs solar irradiation and re-emits in the mid-infrared region that overlaps with the absorption spectrum of aqueous ILs; mid-IR wavelengths correspond to thermal emission from a blackbody heated to temperatures ~100 °C.

To demonstrate the feasibility of this new draw regeneration mechanism at the lab-scale, diluted draws of TFA and DMBS from FO desalination of produced water feeds were each tested with the photonic heater (comprising a selective solar absorber and a blackbody emitter, fig. S15), as shown in Fig. 5B. Under an illumination of 1000 W m^{-2} (one-sun solar flux), the absorber temperature rapidly increases to 80 °C as incident sunlight is converted into thermal radiative energy. This heat is transferred to the emitter, causing it to emit as a blackbody at a peak wavelength of ~8 μm matching the spectral absorption profile of IL-water mixtures (fig. S16B). This radiative coupling allows for direct absorption of thermal emission by the underlying liquid, resulting in a temperature increase well-above the LCST, as shown in Fig. 5C. To quantify the extent of phase separation, aliquots of the heated mixture were analyzed for their composition, where the top layer comprises the water-rich phase and bottom layer is the IL-rich phase as shown Fig. 5D. Residual amounts of IL ~10 wt% in the water-rich phase can be removed by a nanofiltration (NF) post-treatment process with a small external pressure input, and the IL-rich phase >65 wt% can be reused as draw in the FO module, as shown in Fig. 5E. We note that an NF polishing step is required to obtain high purity water (<2 wt% IL) as heating alone does not remove IL aggregates from water as shown in the MD simulations; new IL chemistries that exhibit a very

broad phase diagram would be able to eliminate this step, as would end-use applications that do not require ultraclean product water. The pressure required for NF is dictated by the osmotic pressure of the water-rich phase, which was measured in Fig. 2C as ~10 bar, and hence a pressure of 12 bar was applied. Analysis of the NF permeate reveals near-perfect rejection of both ILs, with a water content of 100 wt% for DMBS (owing to its larger size) and 98.8 wt% for TFA, as shown in Fig. 5F. High purity product water is obtained post NF, with a TDS <500 ppm for both IL draws (220 ppm for DMBS permeate and 430 ppm for TFA permeate) that satisfies the maximum contamination level target set by the U.S. Environmental Protection Agency for drinking water (for full water analysis assessment see table S2).[39] These experiments are the first demonstration of utilizing solar heat for regeneration of IL-based draws after produced water desalination, yielding high-quality water for beneficial reuse.

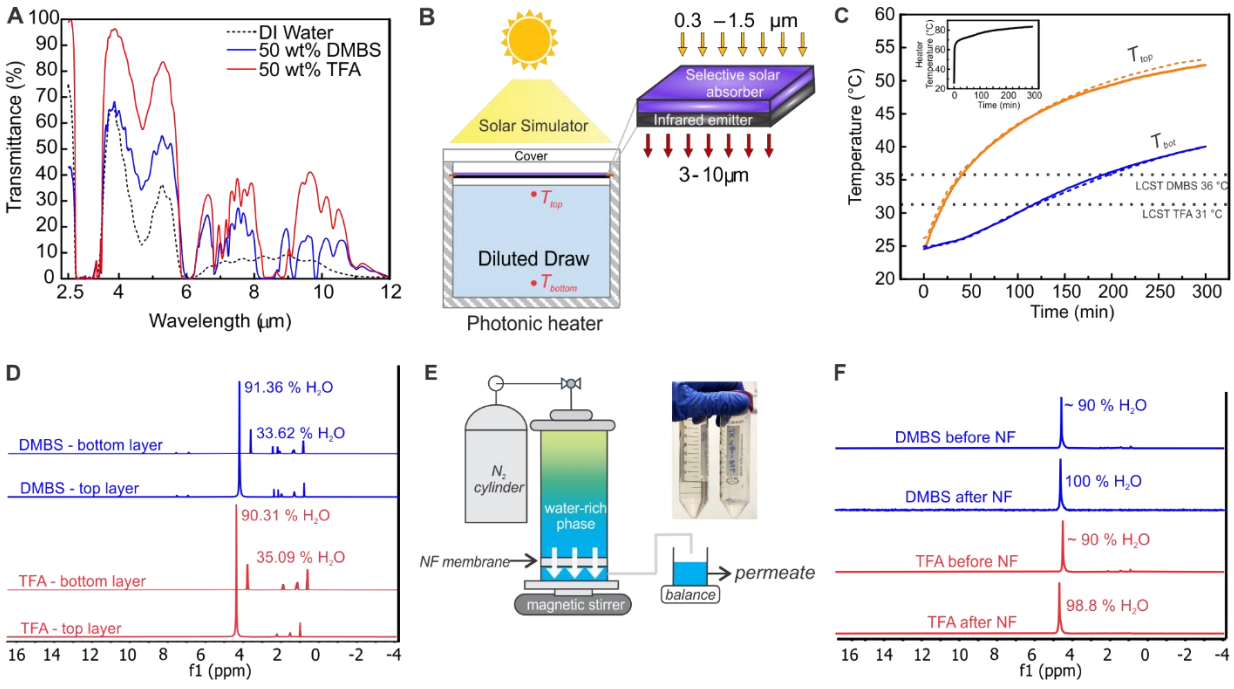

Fig. 5. Experimental testing of draw regeneration using a photonic heater that converts solar energy into infrared radiation for heating above the LCST. **(A)** Optical transmittance of aqueous IL mixtures measured using a 50 μm spacer or path length showing absorption at mid-infrared wavelengths; for larger

path lengths ~1 mm (liquid layer thickness), there is complete absorption across the entire IR range. **(B)** Schematic of a lab-scale setup for radiative heating of diluted IL mixtures using a photo-thermal converter under a solar simulator output of 1000 W m^{-2}. **(C)** Temperature evolution of the diluted DMBS (dashed line) and TFA (solid line) solution, with phase separation caused by radiative heating above their respective LCST; inset shows the temperature profile of the photonic heater. **(D)** ^{1}H-NMR analysis of the water content of the phase separated layers due to solar heating, with the water-rich layer on top of the IL-rich layer. **(E)** Lab-scale setup of dead-end nanofiltration for removal of residual IL from the water-rich phase after solar separation; inset shows the NF permeate after solar-FO of produced water feed (South Mountain) with 70 wt% DMBS and TFA draws. **(F)** ^{1}H-NMR analysis of the water content of permeate from nanofiltration showing near-perfect rejection of ILs at an applied pressure of 12 bar.

Phase separation experiments under realistic conditions of varying solar flux were performed under natural sunlight in Berkeley, California (Supplementary Note S6). These results confirm that temperatures above LCST are attained to induce phase separation of water from the IL (fig. S22), thereby demonstrating the feasibility of such a solar-IL-FO desalination system for regions that have a solar resource ~5 kWh m^{-2} day^{-1} (*e.g.* western United States).

Energy Consumption of Lab Prototype. One important metric for solar-IL-FO is the specific energy consumption of the overall desalination process. As shown in Fig. 1, an integrated solar-FO system comprises draw dilution in the FO module (commercially available from different vendors) and draw regeneration in the thermal separator (custom designed based on draw solution properties). Given that the FO step is spontaneous, the only energy input required at this stage is electricity for circulating feed and draw solutions, estimated as 0.5 - 1 kWh_e m^{-3} (kWh electric) based on previous studies[40] and viscosity of the IL draws. If high-quality product water is desired, a nanofiltration post-treatment can be used to reject residual ILs using electricity. For the experimental conditions shown in Fig. 5, NF with an applied pressure of 12 bar consumes ~0.3 kWh_e m^{-3} (Supplementary Note S7), which yields an overall electrical energy consumption of

<1.5$_e$ kWh m^{-3}. Such a small value is because the primary energy consumption in a solar-IL-FO system is thermal energy required for phase separation of the IL-water mixture by heating. Based on the enthalpy of mixing/de-mixing of the diluted draw (ΔH_{mix}), this is estimated to be 2.7 kWh$_t$ m^{-3} (kWh thermal). Additional energy ~32 kWh$_t$ m^{-3} in the form of sensible heat is required to attain temperatures above LCST for phase separation (52 °C in this case); this results in a total thermal energy consumption of 35 kWh$_t$ m^{-3} for the experimental conditions shown in Fig. 5C, which is provided by a constant solar input of 1000 W m^{-2}. A major portion of this thermal energy consumption is from sensible heating, which is stored in the liquid and can be reused to pre-heat diluted draw before it enters the thermal separator. Taking this into account, the specific thermal energy consumption is calculated to be 9 kWh$_t$ m^{-3} (Supplementary Note S7). This is significantly lower than conventional thermal desalination processes that require 660 kWh$_t$ m^{-3} for evaporating water, as well as highly efficient configurations of multi-effect distillation (MED) with heat recovery that lowers the energy consumption to ~70 kWh$_t$ m^{-3}.[11-12] This highlights the advantage of using draws with novel phase transitions, such as the reversible LCST behavior in thermo-responsive ILs. The energy consumption (both thermal and electrical) is dependent on the diurnal nature of solar irradiation which changes the temperatures of the photonic heater and diluted draw (table S9).

Solar-thermal Efficiency for phase separation. Another important metric for solar-IL-FO is the solar-thermal separation efficiency (η), which dictates the design of the separator. This efficiency is defined as:[36]

$$\eta = \frac{\dot{m}(C_P \Delta T + \Delta H_{mix})}{q_{solar} A} = \eta_1 \times \eta_2 \quad (2)$$

where $\dot{m}$ is the mass flow rate, C_P is the specific heat capacity of the diluted draw (approximated as water), ΔT is the difference between the initial and final temperatures of the mixture; ΔH_{mix} is negligible compared to $C_p \Delta T$, A is photonic heater area, and q_{solar} is the incident solar flux.

There are two parts to this efficiency: η_1 represents the photo-thermal conversion efficiency of the heater (*i.e.,* the efficiency of capturing sunlight and converting it into IR), and η_2 represents the radiative coupling between the heater and the underlying liquid, as well as the absorption efficiency of the IL-water mixture (*i.e.,* the efficiency of utilizing the captured energy for phase separation). These efficiencies guide the design of the two sub-components of the separator. Maximizing η_1 necessitates the use of a selective solar absorber with a high solar absorptance and low thermal emittance that converts incoming sunlight into heat, as well as an emitter with a high infrared emittance that radiates to the underlying liquid. The spectral properties of the selective solar absorber and the blackbody emitter demonstrated in this work satisfy these criteria to yield a photonic heater efficiency of $\eta_1 \sim 91\%$ owing to optical losses by reflection and thermal emission from the selective absorber surface (fig. S15). Maximizing η_2 requires strong radiative coupling between the emitter and liquid, which is achieved with a radiation view factor close to unity and minimal thermal losses (*e.g.* convection from the heater and liquid surfaces and conduction to the walls of the vessel). Maximizing η_2 also requires emission from the heater to be matched with spectral properties of the IL-water mixture. A view factor ~0.8 was achieved in this work by placing the heater close to the surface of the liquid, and spectral property matching was made possible by blackbody emission at 80 °C (temperature attained by the photonic heater in lab experiments) with a peak wavelength ~8 μm that overlaps with measured absorption profile of the liquid (fig. S16). As thermal losses cannot be measured experimentally, a 2D multi-physics model was developed to estimate losses and determine η_2 (Supplementary Note 8 and table S10). This

model reveals that convection losses from the top surface of the heater and absorption of emitted heat by the liquid result in η_2 ~55%. As a result, the overall solar-thermal separation efficiency is 50%, which can be optimized further with design modifications. For example, higher heater temperatures can be attained by reducing convection losses from its surface (*e.g.* using insulation, multi-layer convection shields, vacuum), which consequently increases the radiative power incident on the IL-water mixture. The dimensions of the separator, *i.e.*, its thickness can also be modified to match the thermal penetration depth of incoming infrared radiation, which enables temperatures well-above LCST in under an hour (fig. S23). With these design improvements, a separator efficiency (solar-thermal) of 69% can be obtained due to direct volumetric absorption of radiation by the liquid, which is comparable and even higher than conventional solar collectors operating under similar conditions,[41-42] while also having the added advantage of using noncontact heat transfer. In comparison, heating IL-water mixtures directly with solar energy (*i.e.*, without the photonic heater) would result in an efficiency under 20% due to their poor absorption of sunlight.

ASSOCIATED CONTENT

Supporting Information. The following files are available free of charge: NMR characterization of synthesized ILs; UV-Vis cloud point measurements; DSC enthalpy measurements; MD simulation RDFs; FO water flux reults; SEM images of polymeric FO membrane; EDX analysis of used FO membranes; ATR and FTIR transmission mode measurements; spectral characterization of the photonic heater; NMR analysis of water content post phase separation and NF; outdoor phase separation experiments; specific energy consumption; thermal model; supplementary tables. (PDF)

AUTHOR INFORMATION

Corresponding Authors

* Email: r_kostecki@lbl.gov

* Email: rsprasher@lbl.gov

Author Contributions

†These authors contributed equally.

Funding Sources

This material is based upon work supported by the U.S. Department of Energy's Office of Energy Efficiency and Renewable Energy (EERE) under Solar Energy Technologies Office (SETO) Agreement Number 34324. Work at the Molecular Foundry was supported by the Office of Science, Office of Basic Energy Sciences, of the U.S. Department of Energy under Contract No. DE-AC02-05CH11231. A.K.M acknowledges funding support from the ITRI-Rosenfeld Fellowship from the Energy Technologies Area at LBNL.

Notes

The authors declare no competing interests.

ACKNOWLEDGEMENTS: We thank D. Miller, A. Kisole and E. Lewis from Lawrence Berkeley National Laboratory (LBNL) for assistance with experiments. We gratefully acknowledge Porifera Inc. and Almeco Group for providing FO membrane samples and selective solar absorber samples, respectively, and the California Resources Corporation for providing produced water samples from their oil fields in Southern California.

REFERENCES

1. Urban, J. J., Emerging Scientific and Engineering Opportunities within the Water-Energy Nexus. *Joule* **2017,** *1* (4), 665-688.

2. Rao, P.; Kostecki, R.; Dale, L.; Gadgil, A., Technology and Engineering of the Water-Energy Nexus. *Annual Review of Environment and Resources* **2017,** *42* (1), 407-437.
3. Shaffer, D. L.; Arias Chavez, L. H.; Ben-Sasson, M.; Romero-Vargas Castrillón, S.; Yip, N. Y.; Elimelech, M., Desalination and Reuse of High-Salinity Shale Gas Produced Water: Drivers, Technologies, and Future Directions. *Environmental Science & Technology* **2013,** *47* (17), 9569-9583.
4. Pramanik, B. K.; Shu, L.; Jegatheesan, V., A review of the management and treatment of brine solutions. *Environmental Science: Water Research & Technology* **2017,** *3* (4), 625-658.
5. Tong, T.; Elimelech, M., The Global Rise of Zero Liquid Discharge for Wastewater Management: Drivers, Technologies, and Future Directions. *Environmental Science & Technology* **2016,** *50* (13), 6846-6855.
6. Tow, E. W.; Lienhard V, J. H., Unpacking compaction: Effect of hydraulic pressure on alginate fouling. *Journal of Membrane Science* **2017,** *544*, 221-233.
7. Tow, E. W.; Warsinger, D. M.; Trueworthy, A. M.; Swaminathan, J.; Thiel, G. P.; Zubair, S. M.; Myerson, A. S.; Lienhard V, J. H., Comparison of fouling propensity between reverse osmosis, forward osmosis, and membrane distillation. *Journal of Membrane Science* **2018,** *556*, 352-364.
8. Goosen, M. F. A.; Sablani, S. S.; Al-Hinai, H.; Al-Obeidani, S.; Al-Belushi, R.; Jackson, D., Fouling of Reverse Osmosis and Ultrafiltration Membranes: A Critical Review. *Separation Science and Technology* **2005,** *39* (10), 2261-2297.
9. Thiel, G. P.; Tow, E. W.; Banchik, L. D.; Chung, H. W.; Lienhard, J. H., Energy consumption in desalinating produced water from shale oil and gas extraction. *Desalination* **2015,** *366*, 94-112.
10. Shaffer, D. L.; Werber, J. R.; Jaramillo, H.; Lin, S.; Elimelech, M., Forward osmosis: Where are we now? *Desalination* **2015,** *356*, 271-284.
11. Mistry, K. H.; McGovern, R. K.; Thiel, G. P.; Summers, E. K.; Zubair, S. M.; Lienhard, J. H., Entropy Generation Analysis of Desalination Technologies. *Entropy* **2011,** *13* (10), 1829-1864.
12. Deshmukh, A.; Boo, C.; Karanikola, V.; Lin, S.; Straub, A. P.; Tong, T.; Warsinger, D. M.; Elimelech, M., Membrane distillation at the water-energy nexus: limits, opportunities, and challenges. *Energy & Environmental Science* **2018,** *11* (5), 1177-1196.
13. Kohno, Y.; Ohno, H., Temperature-responsive ionic liquid/water interfaces: relation between hydrophilicity of ions and dynamic phase change. *Physical Chemistry Chemical Physics* **2012,** *14* (15), 5063-5070.
14. Kohno, Y.; Ohno, H., Ionic liquid/water mixtures: from hostility to conciliation. *Chemical Communications* **2012,** *48* (57), 7119-7130.
15. Kamio, E.; Takenaka, A.; Takahashi, T.; Matsuyama, H., Fundamental investigation of osmolality, thermo-responsive phase diagram, and water-drawing ability of ionic-liquid-based draw solution for forward osmosis membrane process. *Journal of Membrane Science* **2019,** *570-571*, 93-102.
16. Cai, Y.; Shen, W.; Wei, J.; Chong, T. H.; Wang, R.; Krantz, W. B.; Fane, A. G.; Hu, X., Energy-efficient desalination by forward osmosis using responsive ionic liquid draw solutes. *Environmental Science: Water Research & Technology* **2015,** *1* (3), 341-347.
17. McCutcheon, J. R.; McGinnis, R. L.; Elimelech, M., A novel ammonia—carbon dioxide forward (direct) osmosis desalination process. *Desalination* **2005,** *174* (1), 1-11.
18. Stone, M. L.; Rae, C.; Stewart, F. F.; Wilson, A. D., Switchable polarity solvents as draw solutes for forward osmosis. *Desalination* **2013,** *312*, 124-129.
19. Hsu, C.-H.; Ma, C.; Bui, N.; Song, Z.; Wilson, A. D.; Kostecki, R.; Diederichsen, K. M.; McCloskey, B. D.; Urban, J. J., Enhanced Forward Osmosis Desalination with a Hybrid Ionic Liquid/Hydrogel Thermoresponsive Draw Agent System. *ACS Omega* **2019,** *4* (2), 4296-4303.
20. Chan, F. T. S., Interactive selection model for supplier selection process: an analytical hierarchy process approach. *International Journal of Production Research* **2003,** *41* (15), 3549-3579.
21. Zhang, Q.; Weber, C.; Schubert, U. S.; Hoogenboom, R., Thermoresponsive polymers with lower critical solution temperature: from fundamental aspects and measuring techniques to recommended turbidimetry conditions. *Materials Horizons* **2017,** *4* (2), 109-116.

22. He, X.; Guvench, O.; MacKerell, A. D.; Klein, M. L., Atomistic Simulation Study of Linear Alkylbenzene Sulfonates at the Water/Air Interface. *The Journal of Physical Chemistry B* **2010,** *114* (30), 9787-9794.
23. Zhou, G.; Liu, X.; Zhang, S.; Yu, G.; He, H., A Force Field for Molecular Simulation of Tetrabutylphosphonium Amino Acid Ionic Liquids. *The Journal of Physical Chemistry B* **2007,** *111* (25), 7078-7084.
24. Liu, X.; Zhang, S.; Zhou, G.; Wu, G.; Yuan, X.; Yao, X., New Force Field for Molecular Simulation of Guanidinium-Based Ionic Liquids. *The Journal of Physical Chemistry B* **2006,** *110* (24), 12062-12071.
25. Horn, H. W.; Swope, W. C.; Pitera, J. W.; Madura, J. D.; Dick, T. J.; Hura, G. L.; Head-Gordon, T., Development of an improved four-site water model for biomolecular simulations: TIP4P-Ew. *The Journal of Chemical Physics* **2004,** *120* (20), 9665-9678.
26. Cornell, W. D.; Cieplak, P.; Bayly, C. I.; Gould, I. R.; Merz, K. M.; Ferguson, D. M.; Spellmeyer, D. C.; Fox, T.; Caldwell, J. W.; Kollman, P. A., A Second Generation Force Field for the Simulation of Proteins, Nucleic Acids, and Organic Molecules. *Journal of the American Chemical Society* **1995,** *117* (19), 5179-5197.
27. Liu, Z.; Huang, S.; Wang, W., A Refined Force Field for Molecular Simulation of Imidazolium-Based Ionic Liquids. *The Journal of Physical Chemistry B* **2004,** *108* (34), 12978-12989.
28. Ionescu, C.-M.; Sehnal, D.; Falginella, F. L.; Pant, P.; Pravda, L.; Bouchal, T.; Vařeková, R. S.; Geidl, S.; Koča, J., AtomicChargeCalculator: interactive web-based calculation of atomic charges in large biomolecular complexes and drug-like molecules. *Journal of cheminformatics* **2015,** *7* (1), 50.
29. Hockney, R. W.; Eastwood, J. W., *Computer simulation using particles*. 1988.
30. Yasukawa, M.; Tanaka, Y.; Takahashi, T.; Shibuya, M.; Mishima, S.; Matsuyama, H., Effect of Molecular Weight of Draw Solute on Water Permeation in Forward Osmosis Process. *Industrial & Engineering Chemistry Research* **2015,** *54* (33), 8239-8246.
31. Kang, H.; Suich, D. E.; Davies, J. F.; Wilson, A. D.; Urban, J. J.; Kostecki, R., Molecular insight into the lower critical solution temperature transition of aqueous alkyl phosphonium benzene sulfonates. *Communications Chemistry* **2019,** *2* (1), 51.
32. Rodríguez, H.; Brennecke, J. F., Temperature and Composition Dependence of the Density and Viscosity of Binary Mixtures of Water + Ionic Liquid. *Journal of Chemical & Engineering Data* **2006,** *51* (6), 2145-2155.
33. Nanda, R., Unusual linear dependency of viscosity with temperature in ionic liquid/water mixtures. *Physical Chemistry Chemical Physics* **2016,** *18* (37), 25801-25805.
34. Yong, J. S.; Phillip, W. A.; Elimelech, M., Coupled reverse draw solute permeation and water flux in forward osmosis with neutral draw solutes. *Journal of Membrane Science* **2012,** *392-393*, 9-17.
35. Achilli, A.; Cath, T. Y.; Childress, A. E., Selection of inorganic-based draw solutions for forward osmosis applications. *Journal of Membrane Science* **2010,** *364* (1), 233-241.
36. Menon, A. K.; Haechler, I.; Kaur, S.; Lubner, S.; Prasher, R. S., Enhanced solar evaporation using a photo-thermal umbrella for wastewater management. *Nature Sustainability* **2020,** *3* (2), 144-151.
37. Cooper, T. A.; Zandavi, S. H.; Ni, G. W.; Tsurimaki, Y.; Huang, Y.; Boriskina, S. V.; Chen, G., Contactless steam generation and superheating under one sun illumination. *Nature Communications* **2018,** *9* (1), 5086.
38. Segelstein, D. J. The complex refractive index of water. University of Missouri-Kansas City, 1981.
39. Office of Water, U. S. E. P. A. *2018 Edition of the Drinking Water Standards and Health Advisories Tables*; Washington, D.C., 2018.
40. McGinnis, R. L.; Elimelech, M., Energy requirements of ammonia–carbon dioxide forward osmosis desalination. *Desalination* **2007,** *207* (1), 370-382.
41. Norton, B., Anatomy of a solar collector: Developments in Materials, Components and Efficiency Improvements in Solar Thermal Collector Systems. *Refocus* **2006,** *7* (3), 32-35.

42. Moss, R. W.; Henshall, P.; Arya, F.; Shire, G. S. F.; Hyde, T.; Eames, P. C., Performance and operational effectiveness of evacuated flat plate solar collectors compared with conventional thermal, PVT and PV panels. *Applied Energy* **2018,** *216*, 588-601.